# Chaotic Trajectories of Tidally Perturbed Inertial Oscillations

NATHAN PALDOR AND EMMANUEL BOSS*

*Department of Atmospheric Sciences, The Hebrew University of Jerusalem, Jerusalem, Israel*

(Manuscript received 15 July 1991, in final form 10 February 1992)

ABSTRACT

It is shown that tidal perturbations of a geopotential height in an inviscid, barotropic atmosphere can turn a purely inertial, predictable trajectory of a Lagrangian particle chaotic. Hamiltonian formulation of both the free, inertial, and the tidally forced problems permitted the application of the twist and KAM theorems, which predicts the existence of chaotic trajectories in the latter case. The chaotic behavior manifests itself in extreme sensitivity of both the trajectory and the energy spectra to initial conditions and to the precise value of the perturbation's amplitude. In some cases dispersion of initially close particles can be very fast, with an $e$-folding time of the rms particle separation as high as one day. A vigorous mixing is induced by the chaotic advection associated with the tidal forcing through the stretching and folding of material surfaces.

## 1. Introduction

Purely inertial trajectories on a geopotential of the atmosphere or the ocean of a rotating earth have been shown by Paldor and Killworth (1988) to consist of entirely predictable oscillations relative to a fixed point on earth. Two conservation laws, for kinetic energy and angular momentum, greatly reduce the dimension of the system's dynamics so that only periodic solutions are possible. A Lagrangian particle flowing along one of these possible trajectories can end up either eastward or westward of the longitude of origin and can either cross the equator or remain in one hemisphere, all depending on the initial velocity and the latitude of origin only. As in many other dynamical systems, the different possible trajectories are separated by the so-called separatrices. The scale for the frequency for all inertial oscillation is twice that of the earth's revolution about its own axis.

A Hamiltonian formulation of a free (i.e., without forcing) dynamical system is of utmost importance in detecting the behavior of the system under the influence of a small-amplitude, time-dependent forcing (Lichtenberg and Lieberman 1983; Wiggins 1988). This Hamiltonian formulation becomes tractable when conservation laws, such as those found by Paldor and Killworth (1988), can be derived. The Hamiltonian formulation of the free system, along with an analogous one for the forced system, enables the application of the Kolmogorov–Arnold–Moser (KAM) theorem to predict the existence of chaos when some external forcing is applied to the otherwise inertial flow.

Many periodic pressure fluctuations perturb any given geopotential surface from its average spherical shape. Of these, two have typical frequencies of the order of the inertial one: the diurnal solar heating and the planetary pressure tide. The solar heating is very well approximated (to an accuracy of a few percent) by a zonally traveling wavenumber 1 and with once- and twice-daily frequencies. The largest components (nearly all the energy) of the planetary pressure tide have zonal wavenumbers one and two and frequencies of once and twice daily, respectively. All these perturbations are called tides because of their frequency range and because it is impractical to try to separate the thermal from the planetary causes of the geopotential height variations. The amplitudes of these tides are latitude dependent but their variation near the equator is very small since they vary as a low power of the cosine of the latitude. The observations (and theories) summarized in Chapman and Lindzen (1970) (see also Haurwitz 1965) and various numerical models (Hsu and Hoskins 1989; Zwiers and Hamilton 1986) give a scale of about 1 mb for the amplitude of these components of the atmospheric surface tide. These tides perturb any given geopotential surface and will act as body forces on all Lagrangian particles flowing along it.

In dynamical systems theory (Wiggins 1988), ample cases exist of linear and nonlinear oscillatory systems that become chaotic when perturbed by some, even minute, time-dependent forcing. This chaotic behavior occurs mostly (but not exclusively) near the separatrices of the free system (e.g., Chernikov et al. 1987, 1988) and is manifested in extreme sensitivity to both

* Present affiliation: School of Oceanography, University of Washington, WB-10, Seattle, WA 98195.

*Corresponding author address:* Dr. Nathan Paldor, The Hebrew University of Jerusalem, Institute of Earth Sciences, Jerusalem, 91904 Israel.

initial conditions and parameter values. A straightforward, in most cases necessary (but never sufficient) tool for detecting the possible existence of chaotic regimes is a direct numerical integration of the system's equations, starting from very close initial conditions or for slightly different values of the parameter; in a chaotic system close trajectories will diverge exponentially. The various time series (and phase plane portraits) that result from these integrations are then analyzed and compared using such tools as power spectra and Poincare maps. These numerical findings have to be supplemented by analytical tools based on the Hamiltonian formulation of both the free and the forced systems. When the systems' Hamiltonians are found the KAM and twist theorems (Ottino 1990) provide conditions under which chaotic behavior is bound to be encountered in the forced system.

The most direct observation on the dispersal of Lagrangian particles in the atmosphere comes from tracking high-altitude weather balloons. In one such field experiment—the EOL Experiment—Morel and Larcheveque (1974) tracked a set of close to 500 balloons released from the ground in several clusters to fly at the 200-mb height. Their main finding was that during the first few days of the balloons' flight their rms separation grew exponentially with an $e$-folding time of over two days. The balloons' dispersal is due, of course, to very many factors, for example, horizontal and vertical shear of the wind at the balloons' altitude and pressure fluctuations other than tides, but the proposition that a great deal of the dispersion is caused by tides has never been considered before. Another such experiment is the TWERL Experiment reported in the TWERLE Team (1977), for which dispersal of balloons was calculated by Er-El and Peskin (1981), who found dispersion rates similar to those found in the EOLE. In addition to the dispersion rates the TWERLE data indicate a nonmonotonic dispersal of the balloons rather than the monotonic dispersal found in the EOL Experiment. The dispersal was heuristically attributed to mechanisms such as Rossby waves, vertical and horizontal shears, and the prevailing winds. Similar observations of the dispersal of submerged floats in the ocean did not yield confident enough dispersion rates due to the sparsity of the data.

We propose an additional mechanism for the observed dispersal that is of wide-range applicability (e.g., satellite and other passive tracers). This mechanism is the dispersion due to chaotic advection of Lagrangian particles flowing on a geopotential when its shape is perturbed by a tidal forcing that induces body forces on the particles. The significance of this mechanism for a given observation should be determined separately since for any original latitude it varies greatly with the initial velocity. Only the combination of these two—original latitude and initial velocity—determines how close the resulting trajectory is to the separatrix. In addition the altitude of the balloon or the mean height of the geopotential determines the amplitude of the tidal forcing so that at higher altitudes the same tidal forcing is expected to result in a wider range of chaotic behavior.

The paper is organized as follows. In section 2 we revisit the free problem by formulating it in a Hamiltonian formulation. In section 3 we present the forcing, and in section 4 the forced problem is cast in a Hamiltonian formulation and we find numerically chaotic trajectories anticipated by the KAM theorem. In section 5 we apply the theory to calculate the dispersion and mixing that are encountered as a result of the chaotic advection. We discuss the applicability of our findings to atmospheric observations and summarize the paper in section 6.

## 2. The inertial problem revisited

The inertial problem—that is, the 2D motion on a geopotential when pressure or viscous forces can be neglected has been studied in the past in connection with trajectories of Lagrangian floats observed in the ocean and as a basic problem in geophysical fluid dynamics (GFD) (e.g., Haltiner and Martin 1957; Von Arx 1962; Cushman-Roisin 1982; Paldor and Killworth 1988). We start off by formulating the problem in the traditional GFD approach but then change to canonical coordinates for a Hamiltonian formulation.

### *a. Review of previous formulation of the problem*

For completeness of presentation we briefly review in this subsection the traditional formulation of the governing equation. More details of the derivations can be found in textbooks such as Gill (1982). The purely inertial (i.e., free), Lagrangian, horizontal equations of motion parallel to a spherical geopotential surface are characterized by the absence of pressure gradient forces and the negligence of viscosity. Buoyancy forces mutually cancel so the shape of the geopotential surface can be assumed to be fixed at all times. When the variation of the Coriolis parameter with latitude and the geometric correction due to the convergence of longitudes are taken into account, one obtains the nondimensional Lagrangian momentum equations for the (eastward and northward) velocity components (see Paldor and Killworth 1988)

$$u_t = v \sin\phi \cdot (1 + u/\cos\phi), \tag{1}$$

$$v_t = -u \sin\phi \cdot (1 + u/\cos\phi), \tag{2}$$

where subscripts (other than zero) denote differentiation. These momentum equations are supplemented by two equations relating the $u$ and $v$ velocity components to the rate of change of the longitude, $\lambda$, and the latitude, $\phi$, respectively:

$$\phi_t = v, \tag{3}$$

$$\lambda_t = u/\cos\phi. \tag{4}$$

In deriving these nondimensional equations the length scale was taken to be $R$—the earth's radius—and the time scale to be 1 day/$(4\pi)$ (i.e., the frequency scale is twice the frequency of the earth's rotation about its own axis). The resulting scale for the velocity components turns out to be $4\pi R/24$ h, which is unphysically large—only slightly less than 1 km s$^{-1}$. We therefore use in all subsequent integrations a nondimensional initial speed of 0.01—a comfortable 10 m s$^{-1}$ dimensional speed.

The absence of $\lambda$ from the rhs of the system (1)–(4) implies that $u$, $v$, and $\phi$ evolve, with time, irrespective of $\lambda(t)$, while the latter is determined by the others. The resulting geophysical trajectories (i.e., relative to a fixed point on earth) $\lambda(t)$, $\phi(t)$ were shown by Paldor and Killworth (1988) to consist of several types of oscillations separated by separatrices. One such trajectory, separating equator-crossing oscillations from those wholly contained in one hemisphere, is shown in Fig. 1.

### b. *Integrals of motion and the system's dimension*

Two integrals of motion were derived for the system (1)–(4) by Paldor and Killworth (1988): The energy integral is obtained by multiplying Eq. (1) by $u$ and Eq. (2) by $v$ and then adding the resulting equations. One then obtains the integral of motion:

$$E_t \equiv (u^2 + v^2)_t/2 = 0, \tag{5}$$

which merely expresses the conservation of the kinetic energy $E$.

The second integral is derived by dividing Eq. (1) through by Eq. (3) and solving for $u(\phi)$. The result is

$$D_t \equiv [\cos\phi \cdot (\cos\phi + 2u)]_t = 0, \tag{6}$$

which expresses the conservation of angular momentum $D$.

These two integrals of motion, $E$ and $D$, along with the independence of the system (1)–(4) on $\lambda$, imply that the dimension of the system is only 1. Indeed, the conservation laws (5) and (6) for $E$ and $D$ can be substituted for $u$ and $v$ to derive (after some tedious but trivial mathematical manipulation) the single, first-order equation:

$$\phi_t^2 = 2E - u^2$$
$$= 2E - D^2/(4\cos^2\phi) + D/2 - \cos^2\phi/4, \tag{7}$$

and this equation is entirely equivalent to the whole system (1)–(4) since once $\phi(t)$ is calculated from Eq. (7), $v(t)$ is given by Eq. (3), $u(t)$ by Eq. (5), and $\lambda(t)$ by Eq. (4). The actual solution for $\phi(t)$ from Eq. (7) for given initial value $\phi(0)$ and particular values of the parameters $E$ and $D$ [determined by the initial values $\phi(0)$, $u(0)$ and $v(0)$] involves elliptic integrals and can be easily obtained numerically. The particular case of the separatrix shown in Fig. 1b ($v(0) = 0$, $D = \cos\phi(0)$, $E = (1 - \cos\phi)^2/8$) can be solved explicitly for $\phi(t)$ (see Boss 1991):

$$\sin\phi = 2\sin\phi(0)\exp(-\alpha t/2)/(1 + \exp(-\alpha t))$$

where

$$\alpha^2 = 1 - D^2.$$

The low dimensionality of the problem and the numerical results showing oscillatory motion only suggest that the system is merely an example of a classical nonlinear oscillator (e.g., Tabor 1989; Lichtenberg and Lieberman 1983). An equivalent equation to Eq. (7) in a more straightforward form can be easily obtained [e.g., by differentiating Eq. (7) with respect to time and dividing through by $\phi_t$, assuming, of course, it does not vanish identically]:

$$\phi_{tt} + V(\phi)_\phi = 0, \tag{8}$$

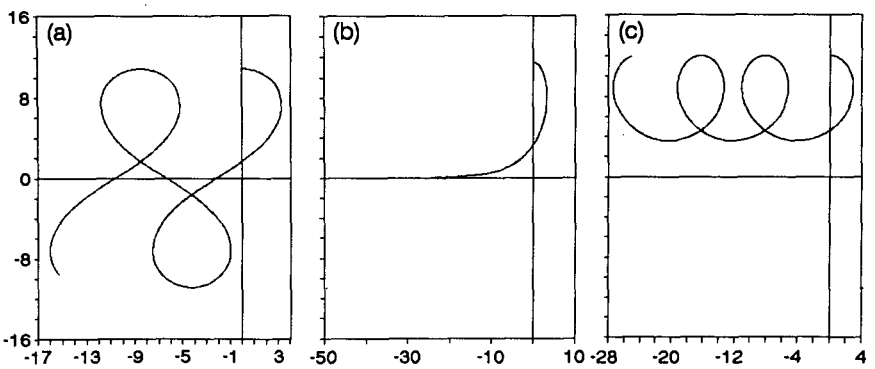


FIG. 1. The inertial (free) trajectories in geopotential coordinates ($\lambda$, $\phi$) for $u(0) = 0.01$, $v(0) = 0.0$ and $\lambda(0) = 0.0$ for three values of initial latitude $\phi(0)$: (a) 0.190 rad, (b) $\cos^{-1}(1 - 2u(0)) \approx 0.20033$ rad, and (c) $-0.210$ rad. The separatrix in (b) separates equator-crossing trajectories from those contained in the hemisphere of origin at all times.

where the nonlinear potential, $V(\phi)$, is defined by

$$V(\phi) = D^2/(8\cos^2\phi) - D/4 + \cos^2\phi/8. \quad (9)$$

The dynamics of this inertial oscillator is determined by the potential, $V(\phi)$, which depends on the value of (the constant) $D$ as shown in Fig. 2. It is clear from this figure that for given initial conditions $\phi(0)$, $\phi_t(0)$ the time evolution of $\phi(t)$ is qualitatively different for different values of $D$. Whereas for $D = 1.5$, only one equilibrium point exists about which the system can oscillate; in the case when $D = 0.5$ there are three such points. This qualitative change in the system's dynamics due to a change in the value of $D$ is better illustrated in the bifurcation diagram shown in Fig. 3. The transition from three equilibrium points (two of which are elliptic and the third being hyperbolic) to one (elliptic) equilibrium point occurs when (the absolute value of) $D$ passes through the value of 1. The system thus undergoes a pitchfork bifurcation at $D = 1.0$ (e.g., particles crossing the equator with zero zonal velocity). For negative values of $D$ the bifurcation diagram is a mirror image of that shown in Fig. 3 since even though $V(\phi)$ (and $H_0$ defined later) contains a linear term in $D$, this linear term is time independent and does not alter the nature of the equilibrium points and the dynamics. This term appears in the expression for $V$ (and that of $H_0$) only due to the choice of reference level of zero kinetic energy.

The rest of this study focuses on trajectories with $D < 1$, that is, those near the separatrix shown as curve $c$ in Fig. 3 (duplicated in geophysical space in Fig. 1b). The dynamical implication of the bifurcation point at $|D| = 1$ is beyond the scope of the present study and is left for future work.

### c. *Hamiltonian formulation of the problem*

The conservation of energy, Eq. (5), and the analogy to a nonlinear oscillator imply that the energy is the system's Hamiltonian when $u$ is replaced by $D$ and $\phi$ [by virtue of Eq. (6)] for canonical representation. The Hamiltonian of the system is thus taken to be:

$$H_0 = v^2/2 + D^2(8\cos^2\phi) - D/4 + \cos^2\phi/8, \quad (10)$$

Note typo above. Inserted /

where $v$ equals $\phi_t$ and $D$ [defined in Eq. (6)] is a constant [determined by the initial conditions $u(0)$, $\phi(0)$]. The coordinates $v$, $\phi$ are indeed canonical and it can be trivially verified that they satisfy:

$$v_t = -H_{0\phi}; \quad \phi_t = H_{0v}. \quad (11a,b)$$

The set (11) for a given value of $D$ and with $H_0$ defined by Eq. (10) is entirely equivalent to the system (1)–(3).

The fact that the system is Hamiltonian justifies the application of twist and KAM theorems to anticipate

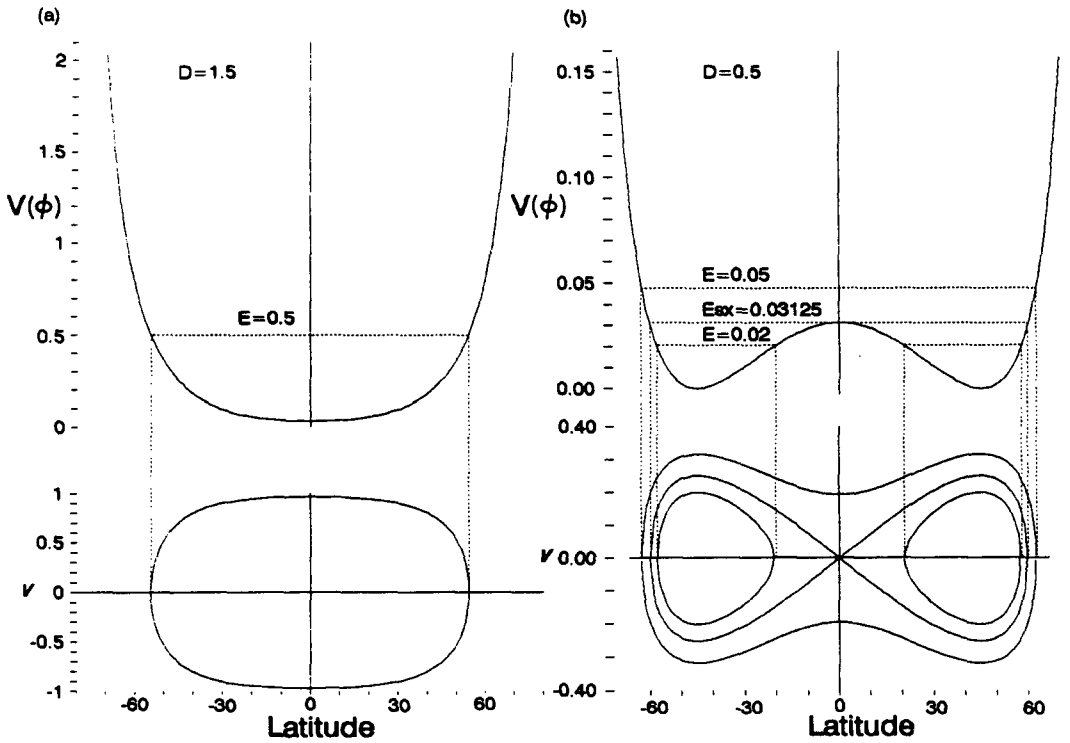


FIG. 2. The nonlinear potential well, $V(\phi)$, governing the dynamics of the free system and the corresponding phase curves $(\phi, v)$ for values of (a) $D = 1.5$ and (b) $D = 0.5$. The transition from a quadratic-looking potential, (a), to a quartic-looking one, (b), takes place at $|D| = 1.0$.

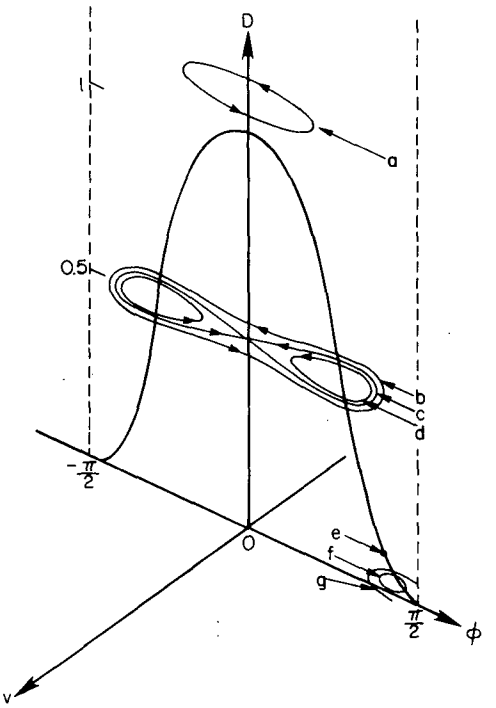


FIG. 3. The pitchfork bifurcation at $D = 1.0$ in $(\phi, v, D)$ space. The various phase space trajectories (a)–(g) shown here are analogous to the geophysical trajectories shown in Figs. 1 and 2 of Paldor and Killworth (1988) with the qualitative correspondence: (a) ⇔ 1a (reproduced here in Fig. 1a); (b) ⇔ 1c, 1d, 1e, 2d; (c) ⇔ 1f (Fig. 1b here); (d) ⇔ 1g (Fig. 1c here); (e) ⇔ 2c (but for $D < 0$); (f) ⇔ 2b; (g) ⇔ 2a. The geophysical trajectory shown in Fig. 1b of Paldor and Killworth (1988) corresponds to a $D = 1$ circle not shown here.

that the addition of a time-dependent forcing will turn some of the free system's oscillatory trajectories chaotic. The extent of chaotic regime is determined by the amplitude of the applied external forcing (Lichtenberg and Lieberman 1983). That same fact also implies that the system is not dissipative and hence that volume in phase space is conserved.

## 3. Tidal forcing

When the geopotential surface along which the Lagrangian particle flows is perturbed by some time-dependent forcing, additional terms have to be added to the rhs of Eqs. (1)–(2). The general form of the dimensional tidal pressure forcing, $p$, is

$$p(\phi, \lambda, t) = a(\phi) \sin(k\lambda - \sigma t), \qquad (12)$$

which represents a zonally traveling wave with a frequency $\sigma$, zonal wavenumber $k$, and latitude-dependent amplitude $a(\phi)$.

Several types of forcing with frequencies near the inertial one come to mind. The main components of the planetary tidal potential are the lunar and solar ones with wavenumbers $k = 1$ and 2 and frequencies $\sigma = 0.5$ (daily) and 1.0 (twice daily). The diurnal cycle of solar heating followed by night cooling, which causes the geopotential to deflect from its mean height, is made up of zonal wavenumber $k = 1.0$ and nearly 95% of the energy is contained in the daily and twice-daily bands. Observations (e.g., Haurwitz 1965; Chapman and Lindzen 1970) as well as numerical models (e.g., Hsu and Hoskins 1989; Zwiers and Hamilton 1986) all indicate the significant role these tidal components play in determining the time series of the geopotential height.

The amplitude of the observed tidal forcing at the surface is nearly 0.6 mb for the daily component and about 1.2 mb for the twice-daily one. The altitude dependence of these amplitudes is such that the diurnal pressure one is slightly increasing with altitude while that of the twice-daily one remains nearly uniform with altitude (Hsu and Hoskins 1989).

The latitude dependence of the observed tidal amplitude, $a(\phi)$, is more complex but to a very good approximation is given for both components by the cosine of latitude raised to a low (two or three) power (Chapman and Lindzen 1970; Hsu and Hoskins 1989).

When the tidal forcing is introduced into the rhs of the momentum equations, Eqs. (1) and (2), we get (e.g., Gill 1982):

$$u_t = v \sin\phi(1 + u/\cos\phi) - kA \cos(k\lambda - \sigma t)/\cos\phi, \qquad (13a)$$

$$v_t = -u \sin\phi(1 + u/\cos\phi) - A_\phi \sin(k\lambda - \sigma t), \qquad (13b)$$

Note typo: no 2.

while Eqs. (3) and (4) remain unchanged. Here the nondimensional amplitude, $A(\phi)$, is defined as the dimensional pressure amplitude, $a(\phi)$, divided by the density and scaled on $(\Omega R)^2$. Thus, a dimensional pressure amplitude of 1 mb (100 Pa) at sea level (density of 1 kg $m^{-3}$) corresponds to $A = 10^{-4}$.

Although the tidal amplitude varies only slightly with height, a main contribution to the variation of $A$ with altitude stems from the density decrease. Therefore, we anticipate that, since $A$ is given by the pressure amplitude divided by the density, its value above sea level should be *higher* than its sea level value of $10^{-4}$.

## 4. The forced model

As was already pointed out at the end of section 2, the addition of even a small-amplitude forcing [e.g., Eqs. (13)] is expected, by the twist and KAM theorems (e.g., Ottino 1990), to turn some of the oscillatory trajectories of the inertial system chaotic. Before turning to the numerical search for these chaotic trajectories, we look at the Hamiltonian of the forced system and derive some important conclusions on its dynamics. In the Hamiltonian formulation of the forced system we will address both time-dependent and time-independent forcing terms having an arbitrary

zonal wavenumber, $k$, and an arbitrary latitude dependence, $A(\phi)$.

*a. Hamiltonian formulation of the forced system*

The dimension of the forced system written in the $(u, v, \lambda, \phi, t)$ is 5. We first reduce the dimension of the system to 4 by noting that both $\lambda$ and $t$ appear only in a linear combination in the expression for the phase of the forcing. Defining a new coordinate,

$$\theta = [\lambda - (\sigma/k)t]/2, \tag{14}$$

we get the following system:

$$\phi_t = v, \tag{15a}$$

$$v_t = \sin(2\phi)(1 - D^2/\cos^4\phi)/8 - A_\phi \sin(2k\theta), \tag{15b}$$

$$D_t = -2kA \cos(2k\theta), \tag{15c}$$

$$\theta_t = D/(4 \cos^2\phi) - (2\sigma/k + 1)/4, \tag{15d}$$

which is equivalent to the system (3), (4), (13a), (13b). The angular momentum, $D$, is not conserved anymore and the time dependence of the forcing introduces an additional dynamical coordinate, $\theta$. The Hamiltonian of the system (15) is

$$H = \frac{v^2}{2} + \frac{D^2}{(8 \cos^2\phi)} - \frac{D(2\sigma/k + 1)}{4} + \frac{\cos(2\phi)}{16} + A \sin(2k\theta). \tag{16}$$

This Hamiltonian being an integral of the flow implies that the system (15) is actually of dimension 3 only despite its deceiving appearance. The additional pair of canonical coordinates (i.e., in addition to $\phi$ and $v$ discussed in section 2) are, of course, $D$ and $\theta$, which can be shown to satisfy

$$D_t = -H_\theta, \quad \theta_t = H_D. \tag{17}$$

The forced Hamiltonian, (16) can be written as the sum:

$$H = H_0 - D\sigma/(2k) + A \sin(2k\theta), \tag{18}$$

where $H_0$ is the Hamiltonian of the free system defined in Eq. (10). As could be anticipated, when the forcing amplitude, $A = A(\phi)$, is set equal to zero $H$ is equal to $H_0$ up to a constant—$D\sigma/(2k)$ [$D$ being a constant when $A$ equals zero by Eq. (15c)]. We also note that this same Hamiltonian is applicable to time-independent forcing by setting $\sigma$ equal to zero in Eqs. (14), (15d), and (16).

The application of KAM and twist theorems to the forced system is justified provided that the Hamiltonian of the latter equals the sum of the Hamiltonian of the free system (up to a constant) and a small, time-dependent term (Lichtenberg and Lieberman 1983). In our problem, the Hamiltonian of the forced system, Eq. (18), satisfies this general form since $D$ itself [the second term on the rhs of Eq. (18)] is made up of a constant term and a time-dependent term that is proportional to $A$ by virtue of Eq. (15c).

*b. Numerical results*

For definiteness we choose in the numerical integrations that follow the form given by Eq. (13) with $k = 1.0$ and $\sigma = 0.5$ so that the particular forcing under study is a zonally traveling wave of wavenumber 1 and with a daily frequency. The amplitude of the forcing was taken to be latitude-independent $A(\phi) = \text{const}$, which makes the calculations somewhat simpler and produces only a negligible error in the 15° band around the equator where the subsequent integrations are carried out.

The region, near the separatrix of the free problem, has been shown in other oscillators to turn chaotic under the application of some time-dependent forcing (Lichtenberg and Lieberman 1983; Chernikov et al. 1987, 1988) and we therefore focus on this region in the search for chaotic trajectories.

For an initial velocity of $u(0) = 0.01$ and $v(0) = 0.0$ (a dimensional speed slightly less than 10 m s$^{-1}$) the separatrix is located at $\phi(0)$ of 11.478°N (0.2003 rad N)—close enough to the equator so that the negligence of the meridional variation of the tidal forcing is justified. The actual original latitude was taken a mere 0.057° (0.001 rad) south of the separatrix and we therefore expect all trajectories to move westward of the original longitude. The original longitude is 0°, which merely sets the phase of the forcing in Eq. (13) to zero at time $t = 0$.

Starting from these initial values [$u(0) = 0.01$, $v(0) = 0.0$, $\phi(0) = 11.421°$, $\theta(0) = 0.0$] and for our particular choice of the forcing wavenumber ($k = 1$) and frequency ($\sigma = 0.5$), very different trajectories were found for two very close values of the forcing amplitude. The first set of integrations had a forcing amplitude of $A = 26 \cdot 10^{-5}$ (the C case), while in the second $A$ was set equal to $27 \cdot 10^{-5}$ (the P case); both amplitude values are well within the observed range, as discussed in section 3.

The geophysical Lagrangian trajectories [$\lambda(t)$, $\phi(t)$] for the two values of the forcing amplitude are shown in Fig. 4 and the projection of the trajectory onto the $(\phi, v)$ plane is shown in Fig. 5. In both figures it is evident that whereas the P trajectory has a very regular periodic appearance, the C case looks very irregular with several cycles not crossing the equator at all.

The difference in the degree of regularity is best addressed by the kinetic energy spectra shown in Fig. 6. Here the difference between the P and the C spectra stands out in a qualitative way: the former consists of isolated sharp peaks at the forcing frequency and its subharmonics, while the latter has only one significant

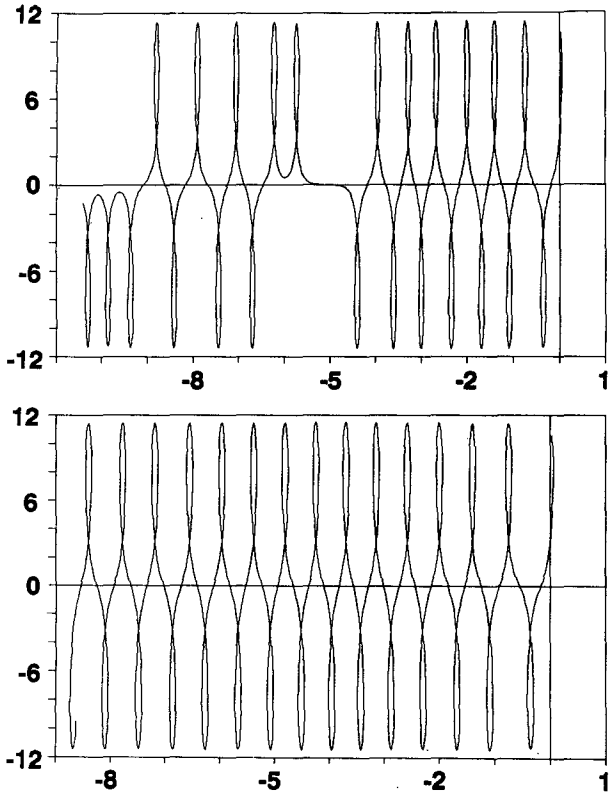


FIG. 4. The geophysical trajectory ($\lambda$, $\phi$) of the forced system for forcing amplitude of: top panel—$A = 26 \times 10^{-5}$; lower panel—$A = 27 \times 10^{-5}$. The trajectory shown in the lower panel (the P case) looks like free oscillation of the type shown in Fig. 1a with very close values for the extreme latitudes since the forcing is weak.

peak at the forcing frequency and the rest of the energy is spread over a wide frequency band.

An additional numerical tool that is often used to prove the existence of chaotic behavior in a dynamical Hamiltonian system is the Poincare map. The Poincare T map acts like a stroboscope that takes a snapshot of the trajectory at a fixed value of the forcing's phase (in our study we chose a forcing phase, $2k\theta = 0$). The advantage of using the map is in that it reduces the dimension of the space necessary for an entirely equivalent description of the dynamics by 1. Thus, in our system, which has a dimension 3 (see section 3), the dimension of the map is only 2. In Fig. 7 we show that the map of the P trajectory is a simple line, while the map of the C case is a complex surface of no simple geometry, the former being typical of a periodic system while the latter is typical of chaotic behavior.

All the indications shown in Figs. 4 to 7 point to the P case being quasi-periodic and the C case being chaotic; that is, not only is it nonperiodic but a complete description of the motion is impractical. This transition from periodic to chaotic trajectories is brought about, for these particular initial conditions, by a minute change—$10^{-5}$ only—in the amplitude of the forcing (corresponding to a relative change of 4% only). These numerical results are merely a demonstration of the chaotic behavior anticipated by the twist and KAM theorems.

We should stress that these numerical results demonstrate only the difference in the *appearance* of these two cases for the particular length of integration used, $O(10^2)$ days, and when the integration is continued for longer times the P case is expected to look more like the C case. Thus, the difference between the two cases should be interpreted as an indication of the sensitivity of the system's evolution over any given finite time interval to the parameter values and not of a fundamental qualitative difference between the two cases. In fact, had we carried out the integrations over a shorter interval, say only up to one third of the length used in Figs. 4–7, then the C time series would have appeared to be as regular as the P series. For sufficiently longer time, on the other hand, the P series can certainly have the irregular appearance of the C case.

## 5. Chaotic dispersion and mixing

A straightforward implication of the chaotic behavior of a dynamical system is its extreme sensitivity to initial conditions even for fixed values of the system's parameters. The results obtained for the dispersion of trajectories emanating from very close initial conditions can thus be compared with observations on the dispersion of passive tracers such as constant pressure weather

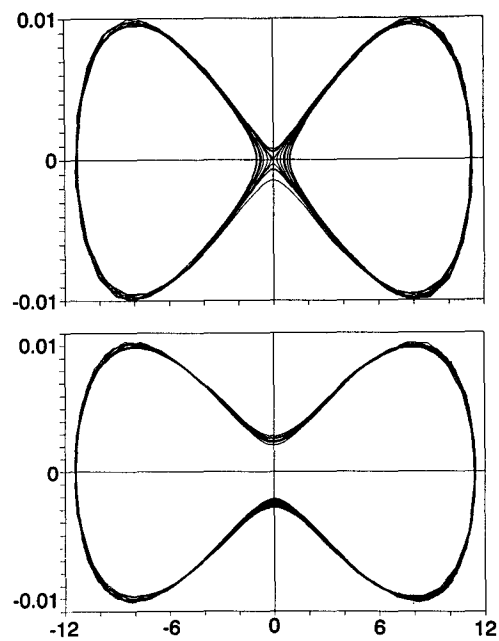


FIG. 5. Same as Fig. 4 but the projection onto the ($\phi$, $v$) plane. The forcing amplitude in both cases is small enough for the maximal velocity to be nearly equal the initial speed. Yet, the slight change in the value of the amplitude causes the oscillatory trajectories in the P case (lower panel) to turn disordered in the C case (top panel).

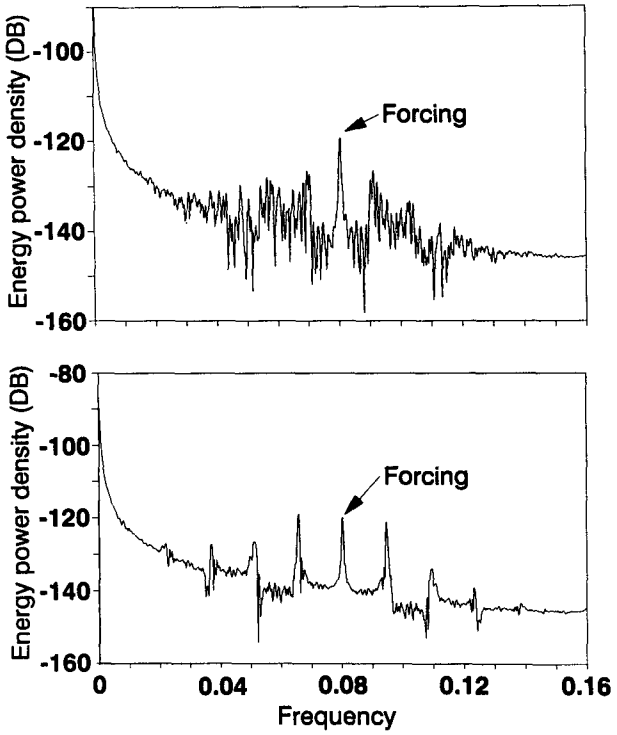


FIG. 6. The spectra of the P case (lower panel) and the C case (top panel). In the C case, no frequency other than the forcing one stands out in the spectrum. By comparison, in the P case subharmonics of the forcing frequency with the inertial one stand out in the spectrum.

balloons in the atmosphere or floats in the ocean. The latter, however, involves too sparse data for a quantitative comparison with our model; therefore we compare, in subsection 5a, our results only with atmospheric observations on the dispersion of constant-level weather balloons.

Another point that can be addressed on the basis of our model is the meridional mixing associated with the stretching and folding of tori in phase space or of material surfaces in geophysical space in the course of evolution of a chaotic dynamical system. This intense mixing owes its origin entirely to the forcing, and purely inertial dynamics will not result in any mixing whatsoever. In subsection 5b we quantify this mixing.

### *a. Dispersion of weather balloons*

Typically, atmospheric weather balloons (and the oceanic floats) are released from the ground/sea surface in clusters designed to fly on a specified geopotential surface. During their several-kilometer flight to the designated surface the balloons/floats disperse horizontally so that when the cluster arrives at the desired geopotential height the balloons/floats are located slightly apart from each other (and we ignore their having somewhat different initial velocities, which adds to the dispersion).

One such atmospheric observation is the EOL Experiment reported in Morel (1970) and Morel and Larcheveque (1974), where high-altitude weather balloons flying in the middle to high latitudes of the Southern Hemisphere were tracked for about two weeks. The 483 balloons were designed to fly at the 200-mb level and during the initial (5 days) phase of the flight their rms separation increased exponentially with an $e$-folding time of 2.7 days. This dispersion has been attributed to several factors, such as the horizontal shear of the prevailing winds and high-frequency fluctuations of the geopotential height. Similar dispersion rates and similarly heuristic reasoning (e.g., Rossby waves) were also suggested for observations during the TWERL Experiment (reported by the TWERLE Team 1977) by Er-El and Peskin (1981).

Our theory on inertial trajectories turning chaotic by tidal perturbations of the geopotential height provides an additional such mechanism. From the outset it is clear that in the real atmosphere many other perturbations exist that cause dispersion. Nevertheless, it is instructive to focus on a single such perturbation, never before considered significant in this respect, and calculate its contribution to the overall dispersion. In calculating the dispersion caused by tidal perturbations

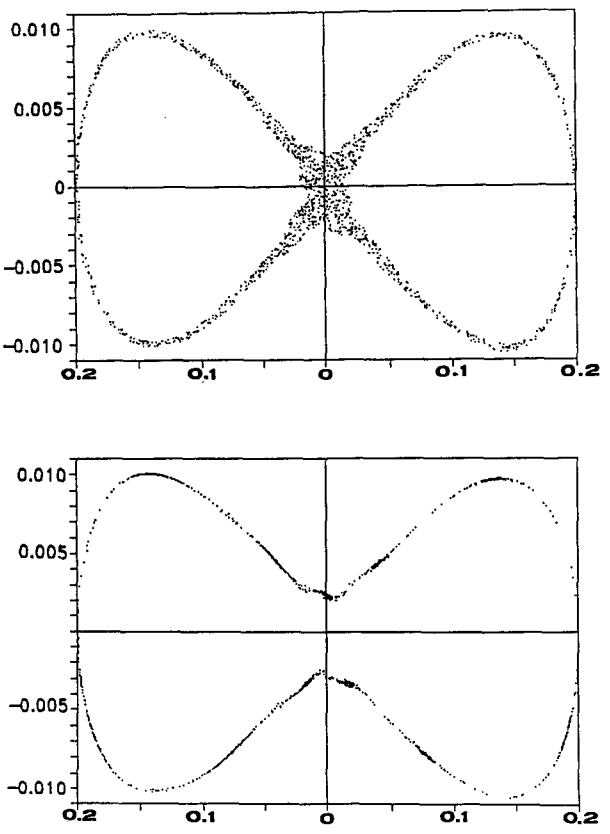


FIG. 7. The $(\phi,v)$ Poincare T map for the P (lower panel) and C (top panel) cases. The maps show the 3D dynamics in the 2D space obtained for zero values of the forcing phase, $\theta$.

only, there is no implication that various causes of dispersion in the atmosphere or the ocean simply add up linearly. On the contrary, the system is highly nonlinear and the exact way in which the various factors add up is extremely complicated and beyond the scope of this work.

In order to assess the significance of tidal mechanism in dispersing tracers flying along a geopotential surface, we have calculated the rate of dispersal of pairs of trajectories emanating from very close initial (spatial) points. In all the trajectories calculated next, the initial conditions for the meridional and zonal velocity components and the values of the forcing's frequency and wavenumber were the same as those used in the preceding section [i.e., $u(0) = 0.01$, $v(0) = 0.0$, $\sigma = 0.5$, and $k = 1$]. The amplitude of the pressure forcing was fixed at the $26 \cdot 10^{-5}$ value used earlier to capture the chaotic trajectories for these initial conditions. The original latitudes and longitudes were randomly chosen from a $10^{-4}$ rad by $10^{-4}$ rad (nearly 0.6 km by 0.6 km) square extending northward and westward of the 11.421°N (0.1993 rad N) latitude and 0.0° longitude point used as the initial point in the preceding section.

Our results for the dispersion of a cluster of 30 inertial pair trajectories forced by our simplified tidal perturbation [Eq. (13)] are shown in Fig. 8. The rms separation of the trajectories increases exponentially during the initial period of nearly 5 days (60 nondimensional time units) with an $e$-folding time of 1.0 day only. By comparison, the rms separation of the free system starting from the exact same initial conditions increases only linearly during that same period

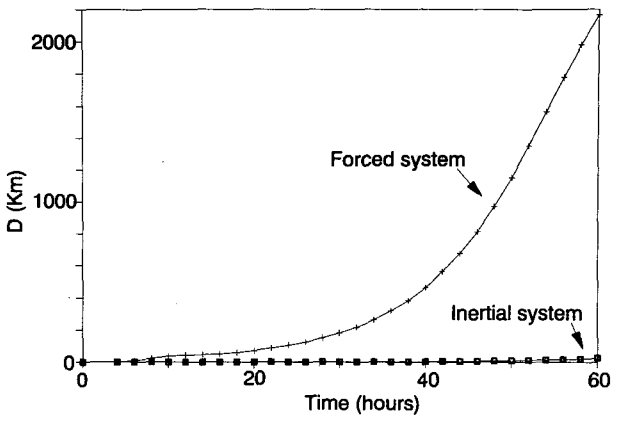


FIG. 8. Root-mean-square separation of model trajectories obtained for slightly (less than $10^{-4}$ rad, i.e., 0.6 km) different initial latitudes and longitudes. Initial conditions are $u(0) = 0.01$, $v(0) = 0.00$, and southwest corner of square of $(\lambda, \phi)$ initial values is at (0.00, 0.1993). The results for the dispersion of the forced system (crosses) best fit an exponential increase with an $e$-folding time of 1.0 day (shown by the solid line), while those for the free system (open squares) best fit a linear increase at a rate of 1.46 km day$^{-1}$ ($r = 0.94$). An exponential best fit of the free system has an $e$-folding time of 0.000 day. For periods other than that used here (60 nondimensional time units) these rates will surely be very different for both the free and the forced cases.

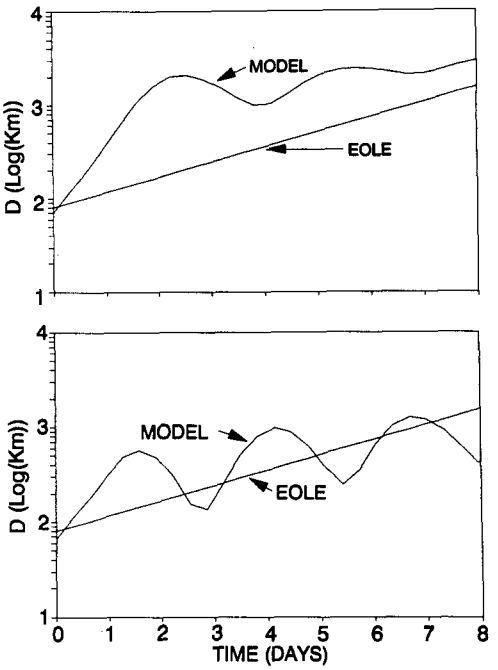


FIG. 9. Model dispersion encountered for trajectories randomly chosen to emanate from an 80-km square centered at $\lambda(0) = 0.0$ and at $\phi(0) = 0.32$ rad—top panel; $\phi(0) = 0.34$ rad—lower panel. The free-system separatrix originates at $\phi = 0.318$ rad for the initial velocity of $u(0) = 0.025$ and $v(0) = 0.00$. Model results are compared with EOLE observations on the dispersion of weather balloons at the 200-mb level. The oscillatory overshooting increase in the model's dispersion was also encountered in the TWERL Experiment.

at a rate of nearly 1.5 km day$^{-1}$. The rapid dispersion of the forced trajectories in our theory does not necessarily imply that passive tracers on a geopotential always disperse at that rate, but merely that they *can* disperse at this high rate given the appropriate combination of original location and initial velocity.

In order to better compare the model with observations, we applied it to initial conditions and tidal forcing more pertinent to the EOL Experiment. The latitude-dependent tidal forcing introduced into the momentum equations in this case had the observed form and values (Haurwitz 1965; Hsu and Hoskins 1989). The initial conditions were $u(0) = 0.025$, $v(0) = 0.00$ (i.e., the free system's separatrix originates at 18.19°), while the initial longitudes and latitudes were randomly chosen from an 80-km long box centered around $\lambda = 0.00$, $\phi = 18.33°$ (trajectories emanating from both sides of the separatrix) in the first run and $\lambda = 0.00$, $\phi = 19.48°$ (all trajectories emanating north of the separatrix) in the second. The dispersion curves shown in Fig. 9 were obtained for the two runs and, as expected, it is evident that when the trajectories emanate from both sides of the separatrix the dispersion is faster, while in the other case the oscillatory overshooting is more pronounced. This oscillatory overshooting following an initial monotonic increase was

observed in the TWERL Experiment reported in Er-El and Peskin (1981).

These encouraging comparisons should be taken as mere indications that the suggested mechanism of tidally forced inertial oscillations might not be negligible in the real atmosphere. Many other forcings interact nonlinearly, with the tidal one resulting in an extremely complicated dispersion.

### b. *Chaotic mixing*

The last geophysical aspect of the chaotic dynamics discussed in sections 3 and 4 is the effect it has on the mixing of material surfaces (or lines) in the atmosphere (or the ocean). This connection between chaotic advection and fluid mixing has been established in many other fluid dynamics and atmospheric problems (Ottino 1990; Pierrehumbert 1991). The chaotic advection of fluid parcels causes efficient stretching and folding of material surfaces, with the net result being that an initially smooth surface stretches throughout the space occupied by the fluid. Another point, besides the rate at which this mixing happens, is the degree of mixing, that is, the fraction of the surface (line) that will actually stretch during the course of the dynamic advection.

A partial answer to both questions is attempted in Figs. 10 and 11, where we calculate the mixing of a latitudinal material line made up of 5760 particles initially spaced $1/16°$ apart (initial conditions: $u(0) = 0.01$, $v(0) = 0.00$, and $\phi(0)$ is set to 0.1993 rad; i.e., $10^{-3}$ rad south of the separatrix at 0.2003 rad; forcing amplitude, $A$, equals $26 \times 10^{-5}$). The stretching and folding of the material line is clearly seen in both ($\lambda$, $\phi$), geophysical space—Fig. 10—and in ($\phi$, $v$), projection of the phase space—Fig. 11. The initial conditions are a straight line in geophysical space and a point in the ($\phi$, $v$) projection of the phase space. To get the mixing rates in units of days, the nondimensional times indicated on the figures have to be divided by $4\pi$. By comparison, the free (inertial) mixing is zero and the initial line merely oscillates northwards and southwards between the latitude of origin and its counterpart in the other hemisphere despite the meridional and zonal motion of the individual material points.

Two points should be mentioned. The first is that the material line stretches monotonically and with time an increasing number of initially close point pairs undergo massive relative displacement. Various pairs of material points that make up the initial line lose their correlation at different times—some are already 1° apart after 90 time units, while others stay highly correlated (i.e., closely packed) even after 180 units. The second point is that even for the small amplitude used here the material line already occupies the entire latitude band (11.47°N to 11.47°S) at $t = 60$ (i.e., less than 5 days) even before the pair correlation is significantly altered.

In general, the way we interpret both dispersion and mixing as resulting from a chaotic stretching and folding of material surfaces is different from the more traditional way of resorting to eddy diffusivity (Kao 1974; Lin 1972) or a modification of that concept (e.g., Bennet 1984). The newly advocated chaotic approach not only provides a well-understood mechanism but, in addition, enables a quantification of the mixing fluxes associated with stretching and folding by several simple numerical algorithms (Swanson and Ottino 1990). There is a fundamental difference between the two mixing processes: the evolution of a chaotic mixing goes from the large scales to the smaller ones, precisely opposite to that of the diffusive mixing (Pierrehumbert 1991; Ottino 1990), which results in a much faster mixing by the former.

## 6. Concluding remarks

Using known techniques from the theory of chaotic mixing in dynamical systems, we were able to study a highly idealized GFD problem relevant to atmospheric Lagrangian dynamics. The crux of this study is that even the small tidal signal in the upper troposphere can, but not always will, cause very efficient mixing and dispersion of an otherwise periodic flow. The caveats and limitations associated with this idealized model as well as its applicability to observations in the earth's atmosphere are discussed and summarized in the following subsections.

### a. *Discussion*

Several points need to be addressed for a complete exposition of the subject. The first point is that the nondimensional amplitudes in our model have very realistic values based on the mean density decreasing with altitude while the geopotential deflection and the pressure amplitude associated with the tidal perturbation being nearly constant with altitude. This is also the reason why the tidal temperature signal (which by the perfect gas law is proportional to the pressure signal divided by the density) is actually increasing with altitude in theories (Lindzen 1967) and numerical models (Zwiers and Hamilton 1986) consistent with wind observations (Wallace and Tadd 1974). The tidal velocity signal, on the other hand, is negligibly small in the upper troposphere (less than 0.50 m $s^{-1}$) and in our model these small velocities appear as the very small spread of the extrema of the ordinate in Figs. 5 and 7 (i.e., maximal $v$ values) compared with the unperturbed value of 0.01.

This brings up the second point that needs clarification. The reason why such small additional velocities are able to induce such a rapid mixing and dispersion is, of course, the choice we made in locating our initial conditions (and the subsequent flow) in such close proximity to the separatrix of the free system. We anticipate that the effect of any given tidal perturbation

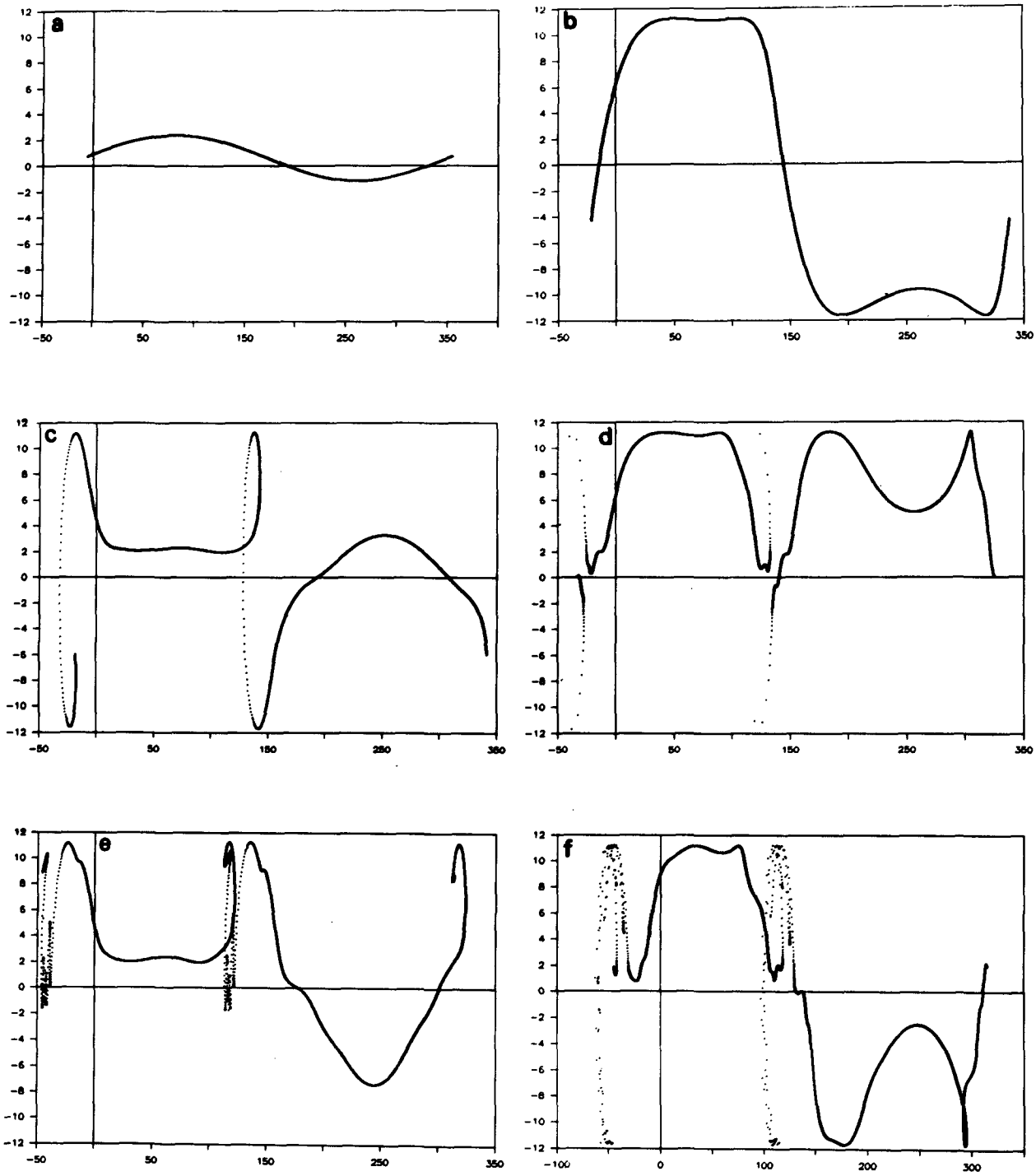


FIG. 10. The change of location ($\lambda$, $\phi$) with time of 5760 Lagrangian particles initially separated by 1/16° longitude in geophysical space. The initial conditions are $u(0) = 0.01$, $v(0) = 0.00$, and $\phi(0) = 0.20$ rad ($10^{-3}$ rad south of the separatrix of Fig. 1b), while the forcing's amplitude is $A = 26 \times 10^{-5}$. The nondimensional times are (a) −30, (b) −60, (c) −90, (d) −120, (e) −150, and (f) −180. The stretching and folding mechanism are very clearly evident in the evolution of this material line.

is much less pronounced in other regions of phase space farther away from the separatrix. Therefore, the phase space contains "islands" of chaotic regimes embedded in "oceans" of essentially periodic ones. The overall density of those chaotic "islands" in phase space is increasing with the tidal amplitude but there are bound

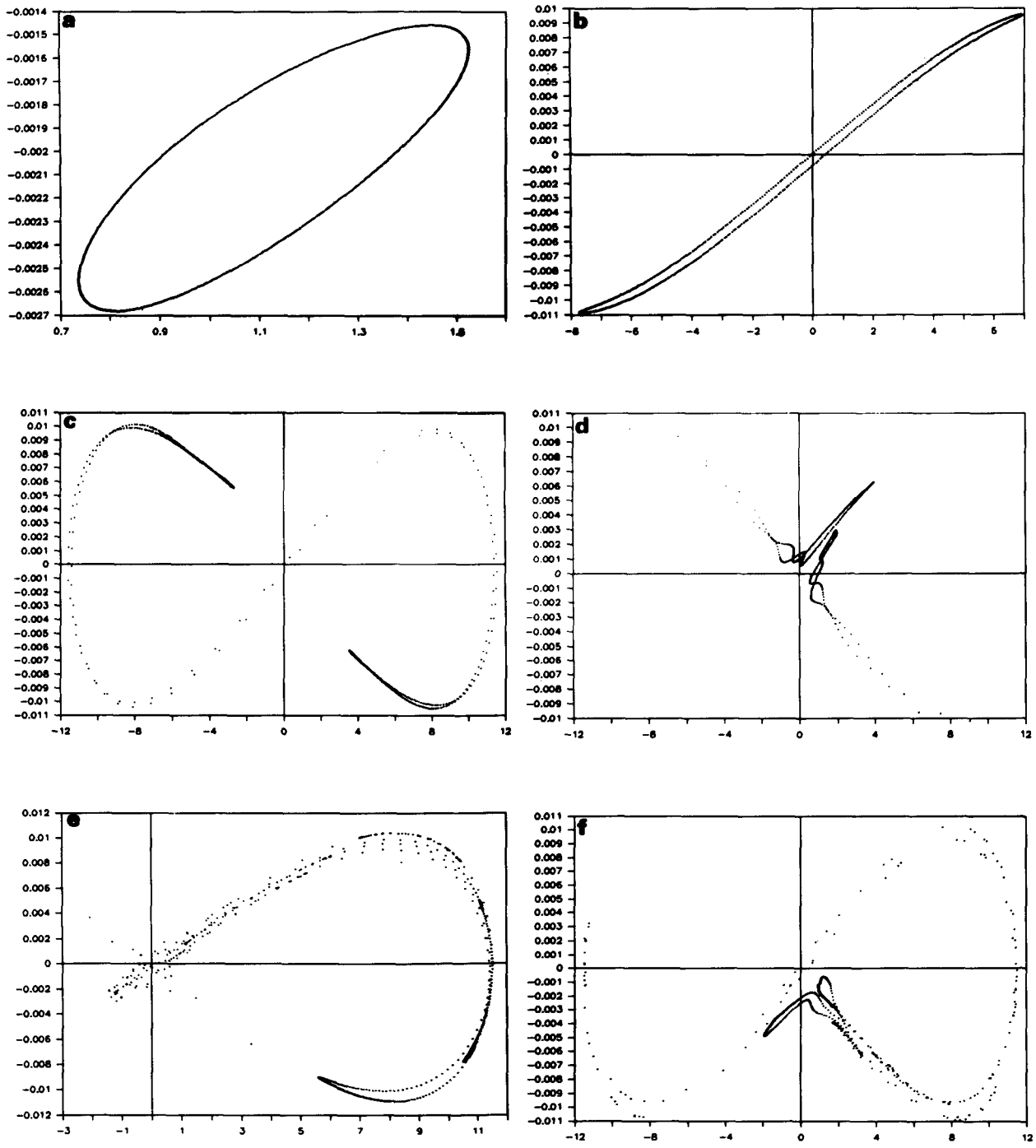


FIG. 11. Same as Fig. 10 but the projection onto the $(\phi, v)$ plane instead of the geophysical space. The stretching and folding are evident here too.

to always exist "seas" of regular flow. Thus, without a global mapping of the phase space and all possible combinations of parameter values our results can not be taken as representative, typical, or average; they should be considered as extreme possibilities with unknown probability of occurrence.

The third point is the effect that other forcings, many of them more potent, that were neglected in our study might have on the observed Lagrangian mixing and dispersion in the atmosphere. As in other nonlinear systems, the mixing and dispersion associated with various forcings cannot simply be added together, and

this interaction of several forcings in a nonlinear system offers a new and challenging problem far beyond the scope of this paper. The inclusion of an additional forcing of the inertial oscillation might reinforce the tidal mixing and dispersion in some parts of the phase space but eliminate it in others. Thus, our results on the mixing by tidal perturbation should be considered as only one piece in a very elaborate puzzle. Mechanistically, however, similar effects are expected to occur for other zonally traveling waves of different amplitudes, wavenumbers, and frequencies. The background very rapid mean flow of the westerly jet is just one such wave, provided its temporal and/or spatial variations are not ignored.

### b. *Summary*

Hamiltonian formulations of both the inertial oscillation problem and its tidally forced counterpart enable the application of the KAM and twist theorems to predict the existence of chaos in the latter. These expectations were actually verified numerically for small amplitude of the tidal forcing.

Very effective meridional mixing and point dispersion can be encountered when even a minute tidal forcing perturbs the inertial flow. The rates of dispersion that can be attained by our model in certain regions of the phase space and for particular values of the parameters are of the same order as the observed dispersion of weather balloons in the upper troposphere. There remain, however, possibly large regions in phase space (and, of course, geographical space) in which the dispersion is only slightly affected by the tidal forcing and the flow is very close to the free one.

These findings should have a significant but quantitatively undetermined effect on the interpretation of data pertaining to dispersion and mixing in the atmosphere (and the ocean) as well as on the construction of eddy terms in GCMs. We were able to tune our model to yield the observed rates of dispersion of weather balloons in the upper troposphere even without resorting to eddy diffusion terms.

Since no complete mapping of the chaotic versus regular regions was attempted (as there are four initial conditions and three forcing parameters in the problem) it is difficult to estimate the globally averaged impact of the tidal forcing on otherwise inertial motion and the role it plays in the earth's atmosphere. Other atmospheric forcings are expected to interact nonlinearly with the tidal one to yield a very complicated and impossible-to-qualify pattern of mixing and dispersion.

*Acknowledgments.* We are grateful to Ms. D. Magen for her enthusiastic help in locating the available experimental data on the subject. Helpful discussions with Dr. V. Rom-Kedar are gratefully acknowledged. The reviewers' comments and suggestions greatly improved this paper.

## REFERENCES

Bennet, A. F., 1984: Relative dispersion: Local and nonlocal dynamics. *J. Atmos. Sci.*, **41**, 1881–1886.

Boss, E., 1991: Inertial motion and chaotic dispersion of Lagrangian particles on a rotating earth. M.Sc. thesis, Hebrew University of Jerusalem.

Chapman, S., and R. S. Lindzen, 1970: *Atmospheric Tides.* D. Reidel, 200 pp.

Chernikov, A. A., R. Z. Sagdeev, D. A. Usikov, M. Yu Zakharov, and G. M. Zaslavsky, 1987: Minimal chaos and stochastic webs. *Nature*, **326**, 559–563.

——, ——, and G. M. Zaslavsky, 1988: Chaos: How regular can it be? *Phys. Today*, **41**, 27–35.

Cushman-Roisin, B., 1982: Motion of a free particle on a beta-plane. *Geophys. Astrophys. Fluid Dyn.*, **22**, 85–102.

Er-El, J., and R. L. Peskin, 1981: Relative diffusion of constant-level balloons in the Southern Hemisphere. *J. Atmos. Sci.*, **38**, 2264–2274.

Gill, A. E., 1982: *Atmosphere-Ocean Dynamics.* Academic Press, 662 pp.

Haltiner, G. J., and F. L. Martin, 1957: *Dynamical and Physical Meteorology.* McGraw-Hill, 470 pp.

Haurwitz, B., 1965: The diurnal surface-pressure oscillation. *Arch. Geophys. Bioclim.*, **a14**, 361–379.

Hsu, H. H., and B. J. Hoskins, 1989: Tidal fluctuations as seen in ECMWF data. *Quart. J. Roy. Meteor. Soc.*, **115**, 247–264.

Kao, S. K., 1974: Basic characteristics of global diffusion in the troposphere. *Advances in Geophysics*, Vol. 18a, Academic Press, 15–32.

Lichtenberg, A. J., and M. A. Lieberman, 1983: *Regular and Stochastic Motion.* Springer-Verlag, 499 pp.

Lin, J-T., 1972: Relative dispersion in the entropy-cascading inertial range of homogeneous two-dimensional turbulence. *J. Atmos. Sci.*, **29**, 394–396.

Lindzen, R. S., 1967: Thermally driven diurnal tide in the atmosphere. *Quart. J. Roy. Meteor. Soc.*, **93**, 18–42.

Morel, P., 1970: Large scale dispersion of constant-level balloons in the southern general circulation. *Ann. Geophys.*, **26**, 815–828.

——, and M. Larcheveque, 1974: Relative dispersion of constant-level balloons in the 200-mb general circulation. *J. Atmos. Sci.*, **31**, 2189–2196.

Ottino, J. M., 1990: Mixing, chaotic advection and turbulence. *Ann. Rev. Fluid Mech.*, **22**, 207–253.

Paldor, N., and P. D. Killworth, 1988: Inertial trajectories on a rotating earth. *J. Atmos. Sci.*, **45**, 4013–4019.

Pierrehumbert, R. T., 1991: Large-scale horizontal mixing in planetary atmospheres. *Phys. Fluids A*, **3**(5), 1250–1260.

Swanson, P. D., and J. M. Ottino, 1990: A comparative computational and experimental study of chaotic mixing of viscous fluids. *J. Fluid Mech.*, **213**, 227–249.

Tabor, M., 1989: *Chaos and Integrability in Nonlinear Dynamics.* Wiley & Sons, 364 pp.

TWERLE Team 1977: The TWERL Experiment. *Bull. Amer. Meteor. Soc.*, **58**, 936–948.

Von Arx, W. S., 1962: *An Introduction to Physical Oceanography.* Addison-Wesley, 442 pp.

Wallace, J. M., and R. F. Tadd, 1974: Some further results concerning the vertical structure of the atmospheric tidal motion within the lowest 30 km. *Mon. Wea. Rev.*, **102**, 795–803.

Wiggins, S., 1988: *Global Bifurcation and Chaos.* Springer-Verlag, 494 pp.

Zwiers, F., and K. Hamilton, 1986: Simulation of solar tides in the Canadian Climate Center general circulation model. *J. Geophys. Res.*, **91**, 11 877–11 896.